nonetheless, well-organized germinal bands formed in about 30% of the cases. Centrifuged control embryos (n = 5) developed normally. Thus, vegetal teloplasm can rescue the ectodermal fate when placed at the animal pole.

From these results, we drew three conclusions about the specification of ectoderm and mesoderm in the leech. First, determinants for these fates are not exclusively localized to the animal or vegetal teloplasm, because both ectodermal and mesodermal precursors can arise in embryos having only animal teloplasm (that is, Vg^x embryos) or only vegetal teloplasm (that is, centrifuged An^x embryos). Second, DAn is competent to become either an ectodermal or mesodermal precursor, whereas DVg seems competent to produce only mesoderm. Third, DAn makes a binary decision between ectodermal and mesodermal fates on the basis of the position of teloplasm along the animal-vegetal axis.

These conclusions are consistent with several models for determination of ectodermal and mesodermal fates. In principle, either the relative or absolute volumes of teloplasm inherited by DNOPQ and DM could specify these fates. However, our measurements of these parameters show only slight differences between conditions that induce ectoderm and mesoderm and thus limit the robustness of any such mechanism. We propose instead that factors imparting ectodermal competence are localized to the animal cortex of the early embryo and thus are stable to teloplasm extrusion and are inherited by DNOPQ, and not DM, at fourth cleavage. We further propose that the ectodermal fate requires a short-range interaction between these cortical factors and teloplasm sometime after second cleavage. In the absence of such an interaction (as in An^x embryos), or in the absence of the factors altogether (as in DM), a mesodermal fate is adopted.

REFERENCES AND NOTES

1. For a review, see E. Davidson [*Gene Activity in Early Development* (Academic Press, New York, 1986)].
2. C. O. Whitman, *Q. J. Microsc. Sci.* **18**, 215 (1878); *J. Morphol.* **1**, 105 (1887).
3. A. P. Kramer and D. A. Weisblat, *J. Neurosci.* **5**, 388 (1985).
4. S. L. Zackson, *Dev. Biol.* **104**, 143 (1984).
5. 2D and 2d by the terminology of K. J. Muller [*Z. Wiss. Zool.* **142**, 425 (1932)].
6. M. Sandig and W. Dohle, *J. Morphol.* **196**, 217 (1988); S. T. Bissen and D. A. Weisblat, *Development* **106**, 105 (1989).
7. D. A. Weisblat, S. Y. Kim, G. S. Stent, *Dev. Biol.* **104**, 65 (1984).
8. D. A. Weisblat and M. Shankland, *Philos. Trans. R. Soc. London* **313**, 39 (1985).
9. J. Fernandez, N. Olea, C. Matte, *Development* **100**, 211 (1987); J. Fernandez and G. S. Stent, *Dev. Biol.* **78**, 407 (1980); D. A. Weisblat and S. H. Astrow, *Ciba Found. Symp.* **144**, 113 (1989).
10. S. H. Astrow, B. Holton, D. A. Weisblat, *Dev. Biol.* **120**, 270 (1987).
11. B. H. Nelson, unpublished observations.
12. B. Holton, S. H. Astrow, D. A. Weisblat, *Dev. Biol.* **131**, 182 (1989).
13. Embryos were obtained from a laboratory colony. *Helobdella robusta* is a species of glossiphoniid leech (M. Shankland, S. T. Bissen, D. A. Weisblat, in preparation) that closely resembles *Helobdella triserialis*, the object of much previous work on this genus.
14. S. S. Blair and D. A. Weisblat, *Dev. Biol.* **101**, 318 (1984).
15. Sectioned embryos were fixed at 4°C overnight in 4% formaldehyde and 0.1 M tris-HCl buffer (pH 7.4), rinsed several times in tris-HCl buffer, dehydrated in an ethanol series, embedded in JB4 embedding resin (Polysciences, Warrington, PA), and sectioned at 14 μm with a glass knife microtome.
16. R. L. Gimlich and J. Braun, *Dev. Biol.* **109**, 509 (1985). RDA was obtained from Molecular Probes.
17. J. Fernandez, *Dev. Biol.* **76**, 245 (1980).
18. Embryos processed for epifluorescence microscopy were fixed for 1 hour at room temperature in 4% formaldehyde in 0.05 M sodium cacodylate buffer (pH 7.3), rinsed and manually devitellinized in 0.1 M phosphate buffered saline (PBS) (pH 7.4), and then incubated at room temperature for approximately 12 hours in each of the following solutions: blocking solution (TBP) consisting of PBS, 2% bovine serum albumin, 1% Triton X-100, and sodium azide (1 mg/ml); a 1:100 dilution of mouse monoclonal antibody to leech nucleus in TBP; several changes of TBP; a 1:250 dilution of fluorescein-conjugated rabbit secondary antibody to mouse antibodies (ICN Biomedicals, Lisle, IL) in TBP; and several changes of PBS. Embryos were then post-fixed for 1 hour at room temperature in 4% formaldehyde with Hoechst 33258 (5 μg/ml) in 0.1 M tris-HCl buffer, rinsed several times in 0.1 M tris-HCl buffer, dehydrated in an ethanol series, and cleared in methyl salicylate.
19. The proportion of embryos in which we failed to achieve complete extrusion of the vegetal teloplasm, as assessed by examination of sectioned zygotes fixed shortly after extrusion, was only 13% (6/45 embryos). This is significantly less than the proportion of Vg^x embryos that developed normally (46% or 30/65), even including in the total those embryos that were discarded because of abnormal early cleavages. Therefore, we rejected the possibility that the 30 Vg^x embryos that developed normally did so because they contained residual vegetal teloplasm.
20. S. L. Zackson, *Cell* **31**, 761 (1982).
21. J. Fernandez and G. S. Stent, *Dev. Biol.* **78**, 407 (1980).
22. The proportion of embryos in which we failed to achieve complete extrusion of the animal teloplasm was 13% (2/16). By the Fisher-Irwin Exact test, this proportion is not significantly different from the proportion of An^x embryos in which DAn exhibited an ectodermal fate (21%). Thus, it is possible that those embryos that formed ectoteloblasts did so because they contained residual animal teloplasm.
23. We measured teloplasm volumes by viewing serial 14-μm sections mounted on microscope slides using differential interference contrast optics with a video camera. The perimeter of the teloplasm was traced with a digitizing tablet connected to a computer graphics workstation (Polycad 10, Cubicomp Corporation, Berkeley, CA). The perinuclear cytoplasm was included in these measurements because it is continuous with and indistinguishable from teloplasm at this stage of development. The area of the polygon was calculated by the computer program and multiplied by the thickness of the section. Volumes obtained for serial sections were then summed. In sections where the teloplasm was not yet completely partitioned between DAn and DVg, a line was drawn through the teloplasm in alignment with the cleavage furrow.

24. We thank S. Bissen, K. Symes, L. Gleizer, R. Kostriken, C. Wedeen, K. Anderson, and J. Gerhart for reading this manuscript and D. Stuart (University of California, Berkeley) for supplying the antibody to leech nucleus. Supported by a postgraduate scholarship from Natural Sciences and Engineering Research Council, Ottawa, Ontario, Canada, to B.H.N. and by NSF grant DCB 87-11262 to D.A.W.

25 January 1991; accepted 26 April 1991

The 2.3 Angstrom X-ray Structure of Nitrite Reductase from *Achromobacter cycloclastes*

J. W. GODDEN, STEWART TURLEY, DAVID C. TELLER, ELINOR T. ADMAN,* M. Y. LIU, W. J. PAYNE, J. LEGALL

The three-dimensional crystal structure of the copper-containing nitrite reductase (NIR) from *Achromobacter cycloclastes* has been determined to 2.3 angstrom (Å) resolution by isomorphous replacement. The monomer has two Greek key β-barrel domains similar to that of plastocyanin and contains two copper sites. The enzyme is a trimer both in the crystal and in solution. The two copper atoms in the monomer comprise one type I copper site (Cu-I; two His, one Cys, and one Met ligands) and one putative type II copper site (Cu-II; three His and one solvent ligands). Although ligated by adjacent amino acids Cu-I and Cu-II are ~12.5 Å apart. Cu-II is bound with nearly perfect tetrahedral geometry by residues not within a single monomer, but from each of two monomers of the trimer. The Cu-II site is at the bottom of a 12 Å deep solvent channel and is the site to which the substrate (NO_2^-) binds, as evidenced by difference density maps of substrate-soaked and native crystals.

NITRITE REDUCTASES (NIRs) ARE part of a denitrification pathway in which nitrate is sequentially reduced to nitrite, nitric oxide, nitrous oxide, and dinitrogen ($NO_2^- \rightarrow NO \rightarrow N_2O \rightarrow N_2$) (*1*). Denitrification is a process that primarily uses energy, occurs anoxically, and has become increasingly important in eutrophic ecosystems (*2*). Denitrification in soil is an important mechanism for loss of plant nutrients and essentially runs counter to nitrogen fixation, and hence is as important a process as nitrogen fixation and photosynthesis in understanding the nitrogen cycle.

J. W. Godden and D. C. Teller, Department of Biochemistry SJ-70, University of Washington, Seattle, WA 98195.
S. Turley and E. T. Adman, Department of Biological Structure SM-20, University of Washington, Seattle, WA 98195.
M. Y. Liu, W. J. Payne, J. LeGall, Departments of Biochemistry and Microbiology, University of Georgia, Athens, GA 30602.

*To whom correspondence should be addressed.

Both heme- and copper-containing NIRs have been described. Copper-containing NIRs (E.C. 1.7.99.3) have been characterized in at least six organisms, the most recent being *Bacillus halodenitrificans* (*3*). The NIR from *Achromobacter cycloclastes* has been reported to be a dimer of total molecular weight of 69,000 with three Cu atoms per dimer (*4*) and most likely having two types of Cu sites (*5, 6*).

Nitric oxide is the product of the reduction of nitrite by *A. cycloclastes* NIR (*4, 5*). This reaction consumes two protons and one electron and has a pH optimum of 6.2 (*7*). The reduction of NO_2^- to NO and the reduction of NO to N_2O are two independent reactions (*8, 9*), although a specific nitric oxide reductase from this organism has not yet been characterized.

A reduced type I blue copper protein (pseudoazurin) was found to be a specific electron transfer donor for the copper-containing NIR from *Alcaligenes faecalis* (*10*). The electron donor to pseudoazurin was ascorbate which, by itself, does not reduce the enzyme. Pseudoazurin from *A. cycloclastes* has also been demonstrated to be able to donate electrons to NIR (*4*). Various cytochromes, including two cytochromes c from the same organism, were not capable of such a reaction, thus demonstrating the specificity of copper-to-copper electron transfer in this pathway (*4*). Furthermore, a detailed study of NIR's kinetics of reduction by pseudoazurin was in favor of a specific interaction between the two proteins. When the concentration of reduced pseudoazurin was higher than that of oxidized NIR, the reduction of the latter occurred in two steps: a burst phase followed by steady-state kinetics. However, when the concentration of pseudoazurin to NIR was 1:1, only the

Table 1. X-ray data collection and phasing statistics. The platinum derivative was made by soaking crystals in 0.1 $K_2Pt(SCN)_6$, 40% saturated ammonium sulfate, 0.1 sodium acetate, pH 5.7, for 4 days. The uranyl derivative was made by soaking native crystals in 4 mM $UO_2(NO_3)_2$, 42% saturated ammonium sulfate, 50 mM sodium acetate, pH 5.4, for 1 day. The major Pt site is bound between molelcules of the trimer, and the eight major uranyl sites are bound to Glu and Asp residues.

Parameter	Data set		
	Native	Pt	U
Resolution (Å)	2.1	2.1	2.2
Data collection			
Unique reflections			
Number	18,163	18,422	16,434
Total possible (%)	90	91*	93
Ratio†	5.7	6.0	4.7
I/σ_I‡	20.7	13.4	8.8
R_{merge} (eq.)§	0.052	0.059	0.070
R_{merge} (sep.)§	0.045	0.055	0.043
R_{nat}		0.15	0.19¶
ΔB‖		2.2	3.8
Sites		3	12
Phasing statistics#			
∞–5.8 Å	0.88	2.5	2.0
5.8–3.8 Å	0.87	2.0	2.2
3.8–3.0 Å	0.76	1.9	2.4
3.0–2.6 Å	0.63	2.1	1.9
2.6–2.3 Å	0.50	2.2	1.5

*Only 61% of all Bijvoet pairs collected. †Ratio of number measured to number of unique reflections. ‡$<I/\sigma_I>$ for highest shell collected. §$R_{merge} = \Sigma|I_i - I|/\Sigma I$; R_{merge} (eq.) Bijvoet pairs treated as equivalent; and R_{merge} (sep.) Bijvoet pairs treated separately. ‖$R_{nat} = \Sigma|F_{deriv} - F_{nat}|/\Sigma F_{nat}$; ΔB is B applied to derivative when scaled to native. ¶R_{nat} only to 2.9 Å. #Figure of merit is given in the native column, ratio of $<|F_{PH} - F_P|>$ to $<E>$, closure error given for each derivative.

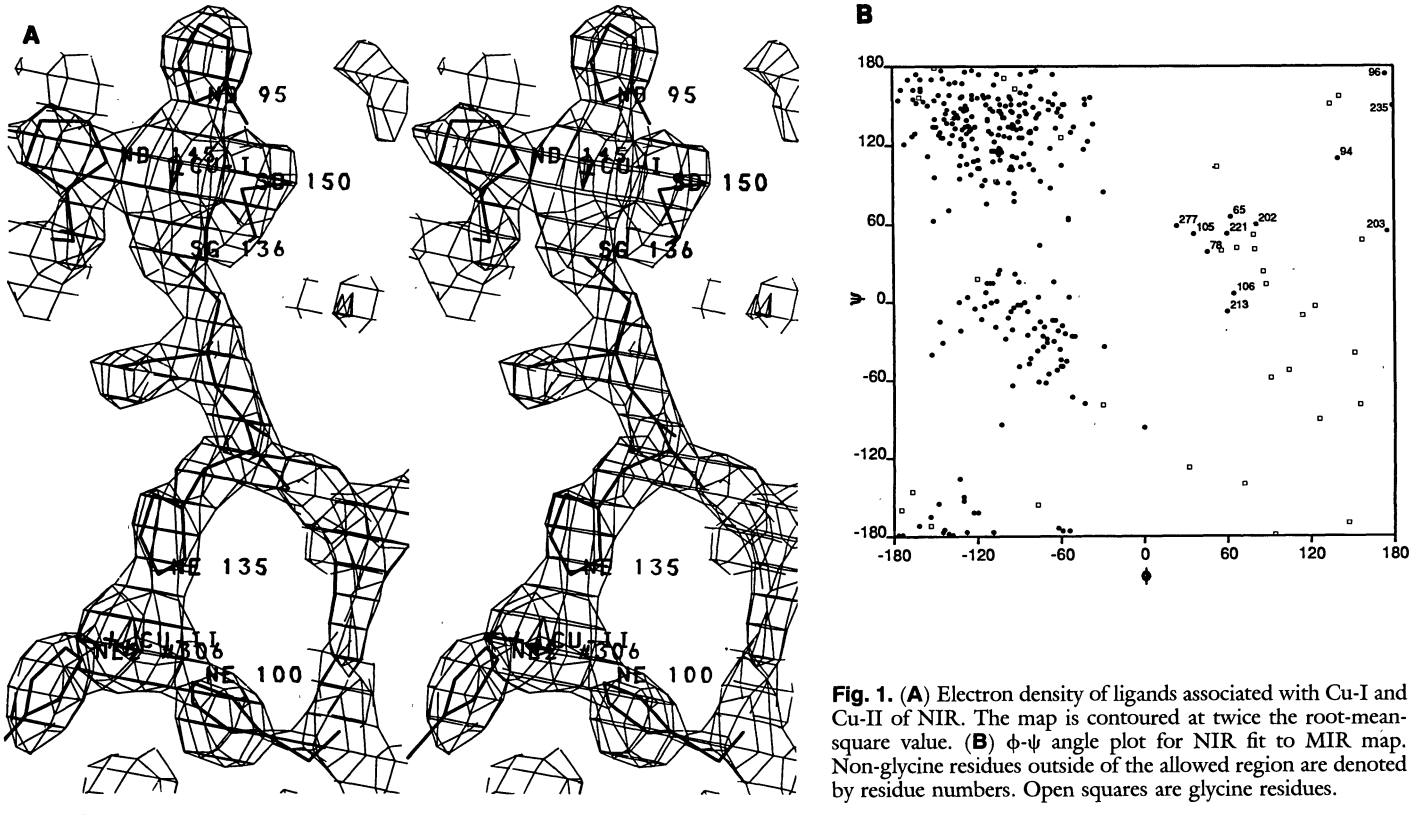

Fig. 1. (**A**) Electron density of ligands associated with Cu-I and Cu-II of NIR. The map is contoured at twice the root-mean-square value. (**B**) ϕ-ψ angle plot for NIR fit to MIR map. Non-glycine residues outside of the allowed region are denoted by residue numbers. Open squares are glycine residues.

burst kinetics was observed (*11*). This specific reaction between the two proteins, in both *Alcaligenes* and *Achromobacter*, is so striking that it has been suggested that the combination of the pseudoazurin and NIR is analogous to the multicopper protein laccase (*10*). Structural studies of NIR were initiated in order to understand how conversion of NO_2^- to NO is accomplished, how NIR can interact with a specific electron transfer partner, and what the nature of the catalytic copper is.

The crystallization of NIR has been reported earlier (*12*). The amino acid sequence (*13*) was fit to a 2.3 Å multiple isomorphous replacement (MIR) electron density map (*14*) on an Evans and Sutherland PS340 system by using FRODO (*15*). Refinement is currently in progress using X-PLOR (*16*). The *R* factor for data from 10 to 2.3 Å is 0.26 after two cycles of positional refinement and one round of refinement with dynamics. The results reported here are based on the model fit to the electron density map.

In the absence of a completely refined structure, several hallmarks (*17*) support the correctness of the present model. Data collection statistics indicate strong phasing power out to 2.3 Å resolution (Table 1). As shown in Fig. 1A, the electron density map is easily interpretable, with no significant gaps and little extraneous connectivity, and the Ramachandran plot (Fig. 1B) shows few residues outside of the acceptable limits. The model produced relates well to proposed homologous structures. With two exceptions, all of the heavy atoms are located near external charged groups. The exceptions are of low occupancy or high *B* value and occur in solvent regions.

Although a monomer is crystallized in the asymmetric unit, the electron density map shows that the monomers are tightly associated around a crystallographic threefold axis and form a trimer. Two β-barrel domains (domain I, residues 8 to 160, and domain II, residues 161 to 340) comprise each monomer (Fig. 2A). The polypeptide fold of both domain I and domain II is a Greek key β barrel, similar to that found for all type I blue proteins (cupredoxins) studied to date (*18*). The two domains are stacked on one another so that the β sheets form a four-layered sandwich with the barrel axes rotated ~40° to each other.

There are two short helical regions, one in each domain. The domain I helix runs from residue 141 to 149 and contains two Cu-I ligands (see below). The domain II helix spans residues 203 to 213. These two helices are sufficiently close that their interaction may stabilize contacts between the domains.

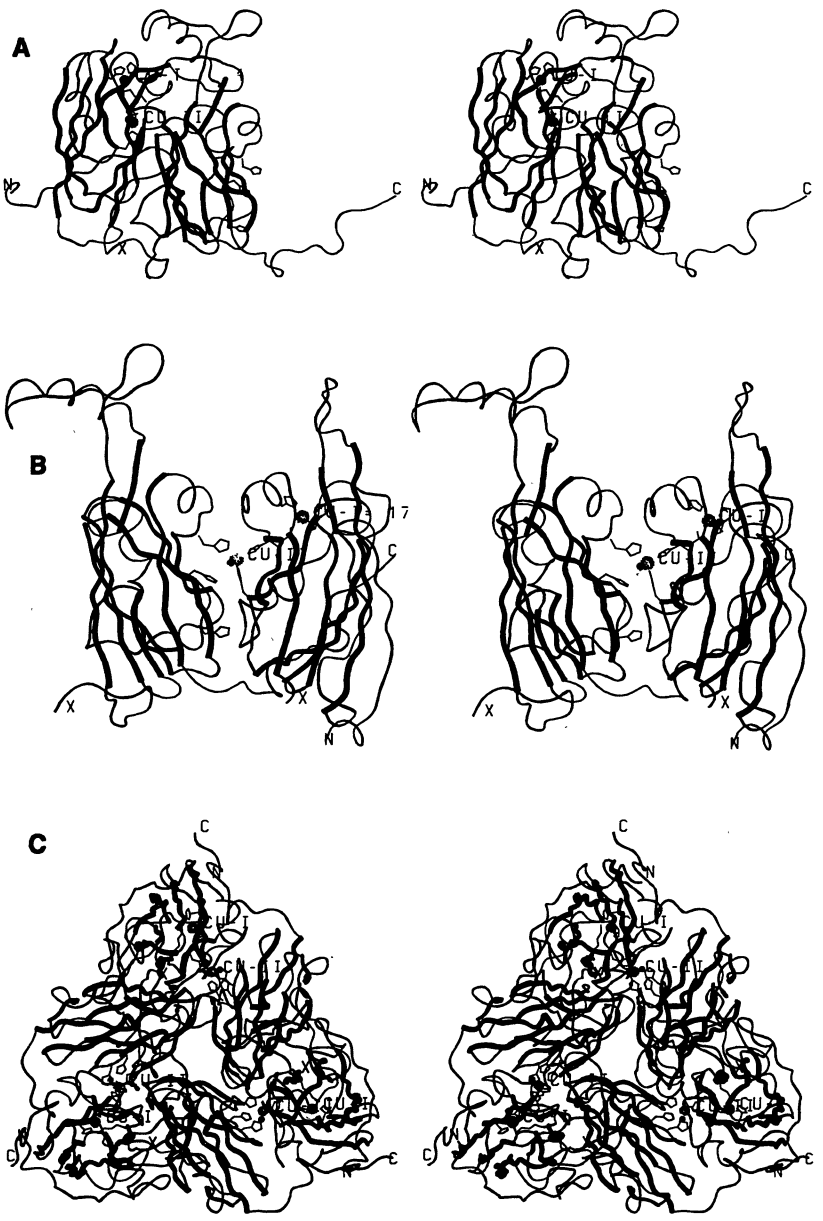

Fig. 2. (**A**) Stereo ribbon drawing of the monomer of NIR. Domain I, to the left, contains Cu-I and His, Cys, His, Met ligands and Cu-II and two of its His ligands. The third ligand to Cu-II comes from domain II of a different molecule. The similarity between domains and to other type I blue copper domains can be seen from the highlighted β-sheet strands. (**B**) Stereo ribbon drawing of the Cu-II site at the interface between domain II of one molecule (domain II′, to the left) and domain I of a different molecule in the trimer. His^{306} is topmost on the left from domain II′. Two non-liganded histidines are also shown; His^{255} is the next one down and, although it cannot be rotated into a ligated position in the present structure, at a higher pH and with a concomitant readjustment of the interface it might. The water ligand is represented as a small dotted sphere in front of Cu-II. (**C**) The trimer of NIR. The interfaces between molecules in (C) run roughly from the chain termini to the central channel.

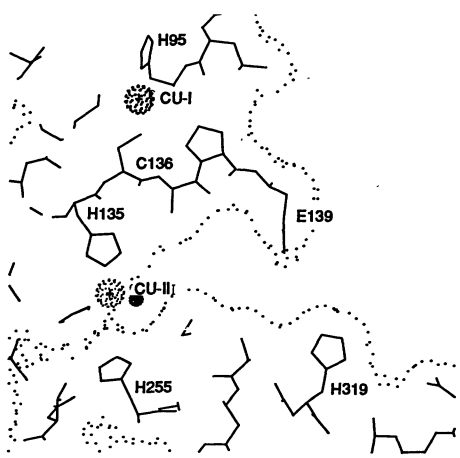

Fig. 3. Solvent access channel to Cu-II. The smaller black dot to the right of Cu-II is the solvent ligand, which appears to be replaced in nitrite-soaked crystals. The edge of the His^{100} ligand is immediately to the left of Cu-II. His^{306} is not visible in the windowing.

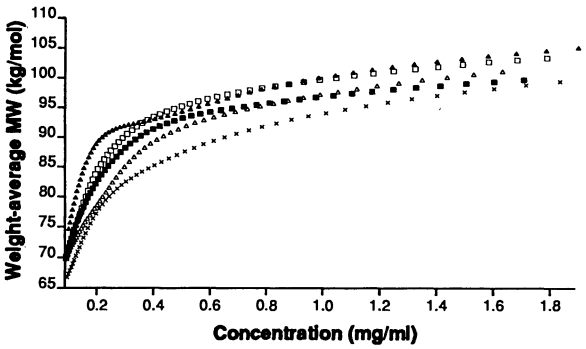

Fig. 4. Weight-average molecular weight (MW) of NIR as a function of concentration determined by sedimentation equilibrium in the analytical ultracentrifuge. The experiment was carried out with three initial loading concentrations of NIR at 18,000 rpm for 22 hours at 5°C. The Rayleigh optical system was used and the data were processed by the methods outlined (*26*). The partial specific volume was calculated from the amino acid composition and corrected to 5°C. The separate curves represent three different sample loading concentrations and replicates of two of them. The third replicate was deleted because of noisy data.

Two extensive loops (the topmost loops in Fig. 2A) interact between domains and provide contacts to other trimers in the crystal. Residues 47 to 62 in domain I provide interactions between domains, and residues 183 to 202 in domain II make contacts between trimers.

The two highest peaks in the electron density map (>8σ) correspond to Cu atoms by virtue of their height and their associated ligands. The two Cu sites are 12.5 Å apart and are bound by adjacent residues in the sequence. All four ligands (His^{95}, Cys^{136}, His^{145}, and Met^{150}) to the first copper come from domain I residues. Since these four ligands (two His, one Cys, and one Met) are normally associated with type I Cu, this first Cu has been labeled Cu-I. Similarly, the ligands to the second Cu (His^{100}, His^{135}, His^{306}, and water) suggest a type II Cu and therefore, it is referred to as Cu-II. The only Cu ligand provided by domain II (His^{306}) comes from a different monomeric unit of the trimer (Fig. 2B). Thus the Cu-II site receives its full complement of ligands only if the protein is a trimer.

The Cu-II site geometry is nearly a regular tetrahedron, whereas the Cu-I could be better described as a flattened tetrahedron or twisted square plane, not unlike pseudoazurin geometry. The Cu-I site lies ~4 Å from the Connolly surface (*19*) of the protein. This distance is deceptively short: a depression at the closest approach is likely to be filled by a solvent molecule, which would make the accessibility similar to that of the type I Cu in azurin. In fact, accessibility to another protein would be further limited by a loop contributed from domain II.

A regular tetrahedron is an unusual geometry for a type II Cu. An electron paramagnetic resonance (EPR) signal with hyperfine splitting constant ≥100 G, and tetragonal or square pyramidal disposition of ligands around the Cu (*20*) characterizes a type II Cu site. In the present molecule the three His ligands are arranged in propeller fashion with the Nε atoms forming a plane ~0.3 Å below the Cu. A type II Cu in NIR was characterized by EPR at pH 6.0, while this structure has been done at pH 5.2. A nearby fourth histidine (255) is definitely not ligated in this structure, but could be at a higher pH.

A central channel spans the trimer's threefold axis (Fig. 2C). This channel is coincident with the monomer's long axis and is ~50 Å in length. Viewed with Connolly surfaces (*19*), the channel is 5 to 6 Å in diameter with a sole constriction of charged residues at the halfway point where the diameter reduces to ~1.5 Å. It is at this constriction that one of the uranyl heavy atoms binds. An unblocked channel of this length calls to mind a membrane pore protein, although the trimer lacks the external band of nonpolar residues characteristic of membrane proteins as seen, for example, in colicin fragment A (*21*). Nonetheless, the interior of the central channel is studded with charged residues that could be involved in proton transport.

Because of the tight trimeric association, the Cu-II site lies deep in a solvent channel formed by two monomers (Fig. 3). This solvent channel or cleft extends 11 to 13 Å from the exterior of the trimer to the Cu-II. The external opening is restricted by Glu^{139} on one side of the channel and His^{319} on the other and therefore may affect substrate access to the Cu. Neither the solvent cleft nor the two Cu sites have direct access to the central channel. The pH optimum of 6.2 observed by Iwasaki (*5*) suggests involvement of a His residue. There are His residues and charged groups positioned between the Cu-II site and the central channel, which suggests a possible proton transfer pathway consistent with the pH optimum observed.

There are three kinds of interactions evident in this structure that would stabilize the trimer in solution: (i) the Cu-II to His^{306} bond; (ii) the extensive intermonomer contact surface surrounding the Cu-II site; and (iii) an extension from domain II that runs outward from residue 324 to the carboxyl-terminus and crosses over to interact with domain I of another monomer of the trimer (Fig. 2C). This last structure, although unusual, is well defined and unbroken in the electron density map.

Since any argument concerning protein association based on a crystal structure is vulnerable to the issue of crystal packing forces and crystallization conditions, we explored the degree of association using a method that examines the native protein in solution. Sedimentation equilibrium experiments were performed with a Beckman Model E analytical ultracentrifuge, and number-, weight-, and *Z*-average molecular weights were determined for NIR in 0.1 M tris and trace amounts of ammonium sulfate at pH 6.8. The monomeric molecular mass was found to be 35,750 g/mol (the amino acid sequence yields a value of 36,451 daltons). There is clear evidence (Fig. 4) of a trimeric species in solution. Stoichiometries of monomer-trimer and monomer-dimer-trimer equilibrium gave equally good fits to the data.

In addition to the structural similarity of each domain to cupredoxins, these domains also resemble those found in ascorbate oxidase (AO) (*22*), a multicopper enzyme with single type I and type II Cu atoms and a pair of type III Cu atoms. The type II and type

Fig. 5. Ribbon drawing of ascorbate oxidase copper-binding domains I and III. The type I site is in domain III to the right; compare with similar orientations of domains II′ and I of NIR in Fig. 2B.

III Cu atoms are in fact arranged in a novel trinuclear cluster, liganded by a total of eight His side chains. There are three β-barrel domains, each with folding characteristic of the cupredoxins. One domain supplies four of the His ligands to the novel trinuclear center, one is devoid of Cu, and the third both binds the type I Cu and supplies four histidines to the trinuclear cluster as well. The β-barrel core of domain I of NIR can be superimposed on domain III of AO. Moreover, with the same rotation and translation, domain II of the neighboring molecule superimposes on domain I of AO. The type I Cu and its ligands in NIR fall at the type I site of AO, and all three of the histidines of the type II site, as well as the Cu, fall in the same site as the trinuclear cluster of AO (Fig. 5). Sequence comparison (*13*) shows that two His from domain I (residues 100 and 135) and two from domain II (residues 255 and 306) correspond to four of the eight ligand His in AO. In NIR only His residues 100, 135, and 306 are ligands. These comparisons suggest that Cu-II of NIR corresponds to one of the type III Cu pair in AO. At an atomic level, the interaction between molecules in NIR resembles the interaction between domains in AO.

The location of catalytic metal at an interface of two otherwise not covalently linked polypeptide chains is rare. One case is the Fe center in the photoreaction center of *Rhodopseudomonas viridis* (*23*). In that case two His ligands come from the L chain and two His and a carboxylate come from the M chain. This Fe center lies deep in that assembly and is not likely to be involved in any interaction with substrate.

Hulse and colleagues have shown that the production of NO or N_2O from this enzyme proceeds through a nitrosyl (E-NO^+) intermediate (*24*). The absence of a fourth protein ligand for the type II Cu suggests that the intermediate would form at this Cu. Suzuki *et al.* (*25*) have reported that the EPR signal of both the *Alcaligènes sp.* (NCIB 11015) NIR (with only type I Cu) and the *Achromobacter* NIR is reversibly lost upon binding NO, suggesting that only the type I site is involved. However, in view of the similarity of the location of the type II Cu to the active site in AO, we believe it is unlikely that the type I Cu in NIR is sufficient for activity. Denariaz *et al.* (*3*) have documented one of the highest specific activities for *A. cycloclastes* NIR.

We have crystallized NIR in the presence of an excess of NO_2^- resulting in a brownish-pink crystal that is isomorphous with the native crystal. Difference density maps showed changes at each Cu site interpretable as NO_2^- displacing the water ligand at Cu-II and a partial loss of Cu at the Cu-I site. A more extensive exploration of these differences as well as a higher pH crystal form of native protein should help further elucidate the mechanism of NIR.

REFERENCES AND NOTES

1. W. Payne, in *Dentrification in the Nitrogen Cycle*, H. L. Golterman, Ed. (Plenum, New York, 1985), pp. 47–65.
2. H. L. Golterman, *ibid.*, pp. 1–6.
3. G. Denariaz, W. J. Payne, J. LeGall, *Biochim. Biophys. Acta* **1056**, 255 (1991).
4. M.-Y. Liu, M.-C. Liu, W. Payne, J. LeGall, *J. Bacteriol.* **166**, 604 (1986).
5. H. Iwasaki, S. Noji, S. Shidara, *J. Biochem.* **78**, 355 (1975).
6. D. M. Dooley, R. S. Moog, M.-Y. Liu, W. J. Payne, J. LeGall, *J. Biol. Chem.* **263**, 14625 (1988).
7. H. Iwasaki and T. Matsubara, *J. Biochem.* **71**, 645 (1972).
8. J. P. Shapleigh and W. J. Payne, *FEMS Microbiol. Lett.* **26**, 275 (1985).
9. J. P. Shapleigh, K. J. P. Davies, W. J. Payne, *Biochim. Biophys. Acta* **911**, 334 (1987).
10. T. Kakutani, H. Watanabe, K. Arima, T. Beppu, *J. Biochem.* **89**, 463 (1981).
11. M. A. Kashem, H. B. Dunford, M.-Y. Liu, W. J. Payne, J. LeGall, *Biochem. Biophys. Res. Commun.* **145**, 563 (1989).
12. S. Turley *et al.*, *J. Mol. Biol.* **200**, 417 (1988).
13. F. F. Fenderson *et al.*, *Biochemistry* **30**, 7180 (1991).
14. The monomer of NIR crystallizes (*12*) in a cubic unit cell, $P2_13$, $a = b = c = 98.4$ Å. Data to 2.0 Å for a native crystal (in a stabilizing mother liquor consisting of 0.1 M sodium acetate at pH 5.2 and 36% saturated ammonium sulfate), and a $K_2Pt(SCN)_6$ derivative were collected at the UCSD area detector facility. A 2.0 Å data set for a uranyl $[UO_2(NO_3)_2]$ derivative was collected on a Siemens area detector in our laboratory. Anomalous scattering data were incomplete for the Pt derivative, so that solvent-flattening methods [B. C. Wang, *Methods Enzymol.* **115**, 90 (1985)] were used to resolve the phase ambiguity. The heavy-atom sites of the uranyl derivative were located from a difference Fourier calculated with these protein phases (Table 1). The uranyl derivative appeared to become non-isomorphous at higher resolution, so phasing was not carried out beyond 2.3 Å.
15. T. A. Jones, *Methods Enzymol.* **115**, 157 (1985).
16. A. T. Brünger, G. M. Clore, A. M. Gronenborn, M. Karplus, *Proc. Natl. Acad. Sci. U.S.A.* **83**, 3801 (1986).
17. C. I. Brändén and T. A. Jones, *Nature* **343**, 687 (1990).
18. E. T. Adman, in *Metalloproteins Part 1: Metal Proteins with Redox Roles*, P. M. Harrison, Ed. (Macmillan, London, 1985), pp. 1–42.
19. M. L. Connolly, *J. Appl. Crystallogr.* **16**, 548 (1983).
20. E. I. Solomon, in *Copper Coordination Chemistry*, K. D. Karlin, and J. Zubieta, Eds. (Adenine, New York, 1983), pp. 1–22.
21. M. W. Parker, F. Pattus, A. D. Tucker, D. Tsernoglou, *Nature* **337**, 93 (1989).
22. A. Messerschmidt *et al.*, *J. Mol. Biol.* **206**, 513 (1989).
23. J. Diesenhofer and H. Michel, *Science* **245**, 1463 (1989).
24. C. L. Hulse, J. M. Tiedje, B. A. Averill, *Anal. Biochem.* **172**, 420 (1988).
25. S. Suzuki *et al.*, *Biochem. Biophys. Res. Commun.* **164**, 1366 (1989).
26. D. C. Teller, *Methods Enzymol.* **27D**, 346 (1973).

27. Supported by NIH grants no. GM31770 and no. GM08268-02. The use of the area detector facility at UCSD is gratefully acknowledged. We thank A. Messerschmidt (Max Planck Institute, Munich) for release of α carbon and copper-ligand coordinates of ascorbate oxidase prior to deposition. The unrefined α carbon, copper, and ligand coordinates of the MIR model of NIR have been deposited with the Protein Data Bank (entry number 1NRD).

5 April 1991; accepted 4 June 1991

Recognition of a Cell-Surface Oligosaccharide of Pathogenic *Salmonella* by an Antibody Fab Fragment

MIROSLAW CYGLER,* DAVID R. ROSE, DAVID R. BUNDLE

The 2.05 angstrom (Å) resolution crystal structure of a dodecasaccharide-Fab complex revealed an unusual carbohydrate recognition site, defined by aromatic amino acids and a structured water molecule, rather than the carboxylic acid and amide side chains that are features of transport and other carbohydrate binding proteins. A trisaccharide epitope of a branched bacterial lipopolysaccharide fills this hydrophobic pocket (8 Å deep by 7 Å wide) in an entropy-assisted association (association constant = 2.05 × 10^5 liters per mole, enthalpy = −20.5 ± 1.7 kilojoules per mole, and temperature times entropy = +10.0 ± 2.9 kilojoules per mole). The requirement for the complementarity of van der Waals surfaces and the requirements of saccharide-saccharide and protein-saccharide hydrogen-bonding networks determine the antigen conformation adopted in the bound state

OLIGOSACCHARIDE EPITOPES OF bacterial and tumor cell-surface carbohydrates are important disease markers (*1*) and targets for therapeutic antibodies (*2*), but to date a crystal structure for an antibody-carbohydrate complex has not yet been reported. Consequently, appreciation of this molecule recognition has been limited to binding site models inferred from functional group replacement in conjunction with immunochemical mapping studies (*3*) and modeling of published binding sites (*4*).

We report the 2.05 Å resolution crystal structure of a carbohydrate epitope bound to a Fab fragment from a mouse monoclonal antibody. The antigen chosen for this study

M. Cygler, Biotechnology Research Institute, National Research Council of Canada, Montréal, Québec H4P 2R2, Canada.
D. R. Rose and D. R. Bundle, Institute of Biological Sciences, National Research Council of Canada, Ottawa, Ontario K1A 0R6, Canada.

*To whom correspondence should be addressed.